JCIM JOURNAL OF CHEMICAL INFORMATION AND MODELING

Computational Biochemistry

Positively charged residues in the head domain of P2X4 receptors assist the binding of ATP

Vanesa Racigh, Agustín Ormazábal, Juliana Palma, and Gustavo Pierdominici Sottile

J. Chem. Inf. Model., **Just Accepted Manuscript** • DOI: 10.1021/acs.jcim.9b00856 • Publication Date (Web): 20 Nov 2019

Positively charged residues in the head domain of P2X4 receptors assist the binding of ATP.

Vanesa Racigh, Agustín Ormazábal, Juliana Palma, and Gustavo Pierdominici-Sottile*

Departamento de Ciencia y Tecnología, Universidad Nacional de Quilmes, Sáenz Peña 352, Bernal B1876BXD, Argentina. Consejo Nacional de Investigaciones Cientficas y Técnicas.

E-mail: gsottile@unq.edu.ar

Phone: +54 (11) 4365 7100 ext 5657

Abstract

P2X receptors are a family of trimeric cationic channels located in the membrane of mammalian cells. They open in response to the binding of ATP. The differences between the closed and open structures have been described in detail, for some members of the family. However, the order in which the conformational changes take place as ATP enters the binding cleft, and the residues involved in the intermediate stages, are still unknown. Here we present the results of Umbrella Sampling simulations aimed to elucidate the sequence of conformational changes that occur during the reversible binding of ATP to the P2X4 receptor. The simulations also provided information about the interactions that develop in the course of the process. In particular, they revealed the existence of a metastable state which assists the binding. This state is stabilized by positively charged residues located in the head domain of the receptor. Based on these findings we propose a novel mechanism for the capture of ATP by P2X4 receptors.

Introduction

ATP-gated P2X receptors constitute a family of non-selective cation channels that are involved in a wide range of physiological processes such as synaptic transmission, taste sensing, immune response, smooth muscle contraction, inflammation, intestinal motility and pain signaling.[1–13] Their malfunction is associated with neurological disorders, cardiovascular problems and cancer.[11,14–18] For these reasons, they hold significant interest as therapeutic targets.[19]

There are seven homotrimeric P2X channels in vertebrates. They are numbered from 1 to 7 ($P2X_1$, $P2X_2$, ..., P2X7).[20] Among them, the only known crystal structures are those of zebra fish P2X4 (zfP2X4),[21,22] human P2X3 (hP2X3),[23,24] panda P2X7,[25] chicken P2X7[26] and rat P2X7.[27] The first structure reported was that of zfP2X4 in the closed conformation. It provided a picture of the overall architecture of the channel and the putative location of the binding pocket. The shape of each subunit was compared to that of a dolphin. The upper part of the chain constitutes the head domain (HD) which is connected, through the body domain (BD), to the transmembrane helices (TM1 and TM2). The BD is also attached to other structural elements called dorsal fin (DF), right flipper (RF) and left flipper (LF). When the three chains are assembled, the entire protein acquires the form of a chalice, whose base is in the intracellular side. The extracellular part presents three deep grooves formed by adjacent subunits. It was proposed that ATP binds to these sites, which are located $\sim$ 45 Å from the TM domains. These features are illustrated in Fig. 1.

Subsequently, the structure of the ATP-bound open conformation of zfP2X4 was revealed.[21] For the first time, it was possible to directly observe the interactions that take place at the docking site. This observation confirmed previous experiments.[28–32] Each ATP binding pocket is formed by two chains, as shown in Fig. 2. For further reference, we named these chains as A and B. The triphosphate tail of the agonist is coordinated by residues Lys316, Asn296 and Arg298 belonging to BD of chain A, and residues Lys70 and Lys72 of BD of chain B. The adenine base of ATP is coordinated by Lys70, Thr189, Leu191 and

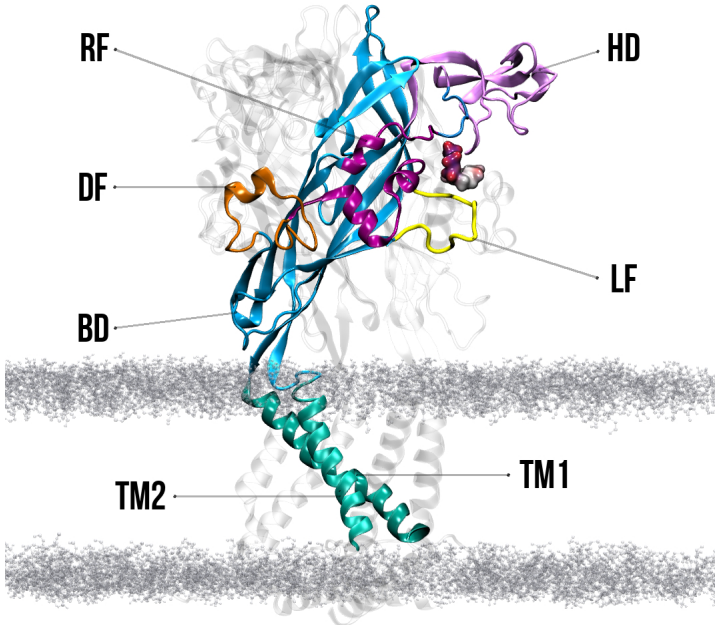

Figure 1: Pictorial illustration of the chains of P2X4 receptors. As suggested by Kawate et. al.,[21] the shape of the chain is compared with that of a dolphin. Different parts are shown with different colors. RF= right flipper, DF= dorsal fin, BD= body domain, HD= head domain, LF= left flipper, TM1 and TM2= transmembrane domains 1 and 2. The location of the binding site in the upper part of the protein is also shown. When the three chains are assembled, the entire protein acquires the form of a chalice.

Ile232 of BD of chain B. Finally, Leu217 is involved in the recognition of the ribose ring. This residue belongs to DF of chain B. The ligand adopts a "U" configuration, with a H-bond between the P_γ phosphate group and the -OH group at the C2* or C3* atoms of the sugar ring.

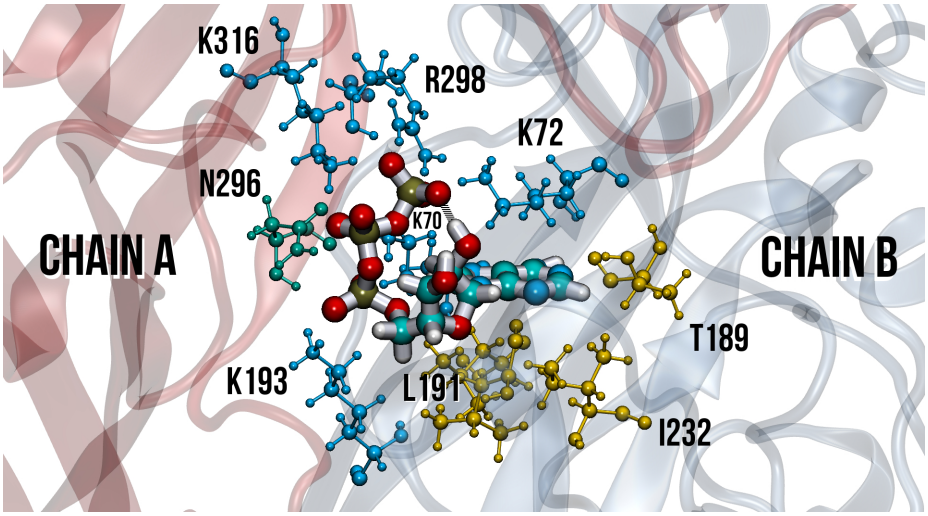

Figure 2: ATP attached to the binding cleft formed by chains A and B. Residues that stabilize the bound conformation are highlighted. Positively charged residues are shown in light blue, polar residues in green and hydrophobic residues in yellow.

The superposition of the closed and open structures afforded a root mean squared deviation of 3.2 Å for the C_α atoms. This demonstrates that the binding of ATP induces significant conformational changes. In addition, the comparison revealed that important interactions are modified throughout this process.[22] Among them, the following are relevant for the subsequent discussion. The switch in the salt bridges of Arg298. This residue strongly interacts with Glu171 in the closed state. In the open conformation, this interaction is missing but Arg298 interacts via salt bridges with ATP.[33] The repulsion between Lys316 and Lys72 that is disrupted when the phosphate tail of ATP enters to the cleft.[34] The approach of His127 to His220 which demonstrates that HD of chain A and DF of chain B approach each other.[34,35]

The functioning of P2X receptors has been the focus of numerous computational studies.[23,36–45] Some of them were devoted to characterize the binding of ATP and the conformational changes that accompany the close-to-open transition. Molecular dynamics simula-

tions and normal mode analysis of the closed structure were used to propose a model for the opening process.[38] Subsequently, MD simulations of the open structure were employed to identify domains that have influence on ATP recognition[37] and receptor activation.[37,46] The dynamics of the closed conformation was analyzed by decomposing its fluctuations into intra-chain deformations and inter-chain movements.[36] Recently, a computational approach was combined with experiments to investigate activation and modulation of hP2X3 by divalent cations bound to ATP. In this study, trajectories in which ATP dissociates spontaneously were generated using a solute-tempering protocol.[41]

Summarizing: major conformational changes that occur along to the opening of P2X receptors, in general, and P2X4, in particular, have already been described. Similarly, the main interactions between ATP and receptor, in the ATP-bound open conformation have been identified. However, the sequence of events by which these conformational changes take place and these interactions develop is still unknown. In this article we present the results of molecular dynamics simulations aimed to shed light on this subject. We have performed umbrella sampling (US) calculations to simulate the reversible unbinding of an ATP molecule from the ATP-bound open P2X4 receptor. The US calculations were complemented with standard molecular dynamics simulations.

From the US computations we estimated the potential of mean force (PMF) for the binding/unbinding process. The analysis of the conformations observed in alternative US windows has revealed how the receptor interacts with ATP and the conformational changes that take place at each stage. This information clarifies the role played by several residues that are known to influence the response of P2X4 to ATP. In addition, we could detect the existence of a metastable state which acts as an intermediary of the binding process. It involves positively charged residues located in the head domain. Based on these findings we propose a novel mechanism for the capture of ATP by the P2X4 receptor.

In the next section, we describe the protocols used to carry out the calculations. The results of the US and standard molecular dynamics simulations are presented after that.

They are followed by a discussion section, where the outcomes of the simulations are put into context and compared with previous experiments and computations. We close the article highlighting the main findings of this work.

Theoretical methods

The US method was employed to simulate the unbinding of a single ATP molecule from the ATP-bound open zfP2X4 receptor. The main assumption of the US approach is that simulations at each US-window are in equilibrium in all directions, except for the movement along the reaction coordinate. Accordingly, when the information from all the windows is taken together, one obtains a description of the process in quasi-equilibrium. In this way, the same simulations provide information for both, the reversible binding and unbinding processes. Besides, standard molecular dynamics simulations were performed for the native P2X4 receptor and its triple mutant, R133A/K136A/R137A, in the closed conformation. These simulations aimed to observe the first stages of the binding process, when ATP recognizes the surface of the receptor and establishes the first interactions.

In the next sections we present the protocols used in this work. First, we describe the procedure followed to prepare the computational model of zfP2X4 embedded in a POPC bilayer. Then, we provide the numerical details of our implementation of the US technique, and discuss the strategies employed to assess the consistency and statistical uncertainty of the results. Finally, we explain how we set the standard MD simulations used to corroborate the existence of a binding site at the head of the receptor.

Model construction and initial settings

The computational model of the receptor was built from the crystal structure of the open form of zfP2X4, PDB entry 4DW1,[22] and the open form of hP2X3, PDB entry 5SVK.[23] The latter contains a significant fraction of the cytoplasmic domain. Thus, we used it as

a template to build the cytoplasmic region of zfP2X4. The details of the procedure have already been provided in Ref. 39. For completeness, we also present them in the Supporting Information of this article. The final model is composed by residues from Ser21 to Thr376. Throughout the article, the numbering of the residues and the names of the atoms correspond to those of the 4DW1 structure.

The protein model was soaked into a square lipid bilayer of 140.0 $Å^2$ with 247 POPC molecules at each side using the graphical interface of the CHARMM membrane builder.[47,48] The channel was displaced along the Z axis in order to align Tyr53 with the top of the membrane. This model was fed into the Leap module of AMBER16. There, it was placed at the center of an octahedral cell of water molecules. Special care was devoted to introduce water molecules into the extracellular vestibule and transmembrane channel. Otherwise, the channel shrinks at the fist stages of the simulation. The system was then neutralized. Finally Na^+ and Cl^- ions were added to achieve a 0.15 M salt concentration. The Amber99SB force field[49] was employed for protein and water while Lipid14 was chosen for POPC.[50] The SANDER and PMEMD modules of AMBER16 were used to run the simulations.[51]

The initial structure was first minimized at constant volume and then heated at NVT conditions from 0 K to 100 K during 120 ps. Next, the heating was continued from 100 K to 303 K during 1.0 ns changing from constant volume to constant presure to allow density to relax. Temperature was controlled with a Langevin thermostat with a collision frequency of 1.0 ps^{-1}. Pressure was controlled with a Berendsen barostat, with a coupling constant of 2.0 ps applying an anysotropic pressure scaling. An harmonic restraint of 1.5 kcal/mol$Å^2$ was applied on the C_α atoms of the protein and the oxygen atoms of the water molecules in the two heating periods. This was followed by four consecutive 10.0 ns simulations at 303 K in which the restraints were gradually diminished (0.5, 0.1, 0.05 and 0.01 kcal/mol$Å^2$). A final equilibration stage of 80.0 ns was performed. The SHAKE algorithm was used to constrain the bonds involving hydrogen atoms. Accordingly, the time step could be set to 2.0 fs. The Particle Mesh Ewald method, with a cutoff radius of 10.0 Å, was employed to

calculate the electrostatic interactions. Therefore, these calculations were done in the direct space for $r < 10$Å, and otherwise in the reciprocal space.[52,53] A cutoff of 10.0 Å was also applied to the rest of the non-bonded interactions.

Umbrella sampling simulations

The starting point of the US simulations[54] was the equilibrated structure of our model of P2X4 in the ATP-bound open state. We defined the reaction coordinate (χ) as the distance between two centers of mass (COM). One of them is the COM of the heteroatoms of the ATP molecule. The other one is the COM of the C_α atoms of residues Thr69-Lys72 and Phe188-Ile192 of chain B, and Asn296-Phe299 of chain A. These residues belong to a rigid part of the upper body that forms the rear wall of the selected binding site. The value of χ was sequentially increased from 8.0 Å to 54.0 Å, with a spacing of 0.1 Å. The last structure of a given simulation was employed as the initial structure of the next one. The force constant of the harmonic bias potential was set to 150.0 kcal/molÅ^2. We checked that for this spacing and force constant, the histograms of the reaction coordinate corresponding to adjacent windows have an appropriate overlap.[55]

We covered the whole range of the reaction coordinate three times. Simulations of different lengths were used each time. Thus, we run simulations of 0.1, 1.0 and 10 ns per US window. Clearly, the shorter simulations are not able to afford quantitatively good results. In spite of this, the qualitative description of the binding/unbinding process is very much the same in the three cases. The PMF presented below was computed with the snapshots taken from the lengthiest simulations, but only the last 8.0 ns of each window were processed. The first 2.0 ns were considered as an equilibration period. The total simulation time employed to calculate the PMF adds up to 4.8 μs.

We implemented two alternative methodologies to calculate the free energy profile from the biased distribution data: the Weighted Histogram Analysis Method (WHAM)[56] and the Dynamic Histogram Analysis Method (DHAM).[57] In both cases, we used our own FORTRAN

codes. The values of the reaction coordinate were binned from 8.0 Å to 54.0 Å using a spacing of 0.02 Å between bin centers. It was hard to get converged results. The WHAM algorithm required 500000 iterations. DHAM could not be used for the complete PMF but for different segments that were then assembled to build the whole curve.

Several assessments were performed to analyze the quality of the PMF. One of them measures the consistency of the data afforded by adjacent simulations. It involves the observation of the following function[58]

$$F_i(\chi) = k_B T \; ln\left(\frac{P_{i+1}(\chi)}{P_i(\chi)}\right) + \Delta U_i(\chi), \tag{1}$$

where k_B is the Boltzmann constant and $T = 303.0$ K. $P_i(\chi)$ and $P_{i+1}(\chi)$ are the probability distributions for χ obtained from simulations i and $i+1$, respectively. $\Delta U_i(\chi)$ measures the difference between the corresponding biased potentials for the given value of χ. As explained in Ref. 58, $F_i(\chi)$ should be almost constant between the centers of adjacent simulations. Thus, we computed $F_i(\chi)$ for all pairs of adjacent windows and verified that such condition was met. A second approach evaluates the consistency between the probability densities truly observed in the US simulations, $P_i(\chi)$, and the biased distributions calculated from the results of WHAM or DHAM, $\mu_i(\chi)$. To that end, we employed the symmetric Kullback-Leibler divergence,

$$S_i = \frac{1}{2}\; D(P_i, \mu_i) + \frac{1}{2}\; D(\mu_i, P_i)\,, \tag{2}$$

where,

$$D(f, g) = \sum_{k=1}^{N} f(\chi_k) \; ln\, \frac{f(\chi_k)}{g(\chi_k)}. \tag{3}$$

Here N represents the number of bins employed in a discretized representation of the probability densities $f(\chi)$ and $g(\chi)$ while χ_k is the value of the random variable at the center of bin k. The lower the value of S_i, the better agreement between the two distributions. Finally, to estimate the statistical uncertainty of the PMF, we divided the data into four equivalent sets, and computed a PMF with each of them. The standard deviation of the

profiles determined in this way was used to estimate the statistical uncertainty of the global PMF, computed from the whole data set.

Standard MD Simulations

The computational models employed in the standard MD simulations were prepared from the PDB structure 3I5D,[21] following guidelines similar to those described above for the open structure. The TLEAP module of AMBER16 was used to build the structure of the mutant from that of the native receptor. For each simulation, a single ATP molecule was added around the extracellular part of the channel. The following protocol was used to establish the initial position of ATP.

We set a coordinate system whose z axis was aligned to the pore axis. The positive direction of the z axis pointed to the head of the receptor. The origin of the coordinate system was defined as the COM of the C_αs of Lys70 of the three chains. This origin is $\sim$40 Å above of the membrane. A 3D grid was set with $x \in$ [-45Å:45Å], $y \in$ [-45Å:45Å] and $z \in$ [-25Å:35Å]. The interval between grid points was 10 Å in each direction. All points in the grid were considered, in principle, as an initial location for ATP. However, some of them proved unrealistic, since they produced clashes between the agonist and the receptor. These locations were discarded. The center of mass of ATP was moved from one grid point to another using US simulations. The procedure afforded 591 alternative initial positions for ATP. These positions are indicated in Figure S1, at the Supporting Information. Each of them was used to launch a standard MD simulation which lasted for 2.0 ns. Snapshots were taken every 4.0 ps. Only the second half of these simulations was employed in the subsequent analysis.

Results

In this section we first present the outcome of the US simulations. After that, we introduce the results of standard molecular dynamics simulations. All the assessments on the accuracy and consistency of the US calculations are presented in the Supporting Information. Fig. S2 compares the PMFs obtained with WHAM and DHAM; Fig. S3 shows typical plots of $F_i(\chi)$ (Eq. 1) while Fig. S4 illustrates the variation of the sKL-divergence (Eq. 3) along the whole range of the reaction coordinate. Fig. S5 shows the PMFs obtained with the alternative sets of data. All these tests afford reasonably good results that validate the findings described below.

To organize the presentation we have divided the whole range of the reaction coordinate into five regions. We discuss separately the observations corresponding to each of them. We have analyzed the variations of several parameters in order to describe the binding/unbinding process. They are depicted in Figs. 3 to 6. Fig. 3 presents parameters that describe the interactions between ATP, receptor and ions. Fig. 4 shows typical conformations of ATP in each of the five regions. Figures 5 and 6 indicate the variation of parameters that describe conformational changes occurring in the extracellular part of the receptor. In particular, panel (a) of Fig. 5 shows the number of H-bonds between the two loops of HD. We found that this number significantly changes along the binding process. Loop 1 goes from Glu121 to Ser128. Loop 2 goes from Asp141 to Val147. Panel (b) indicates the distance between the body domains of chains A and B (BD_A and BD_B) and the torsion between the C_α atoms of residues Leu209, Asn213, Leu217 and Cis230. This angle provides an indication of the torsional movement of DF of chain B. The separation between BD_A and BD_B was estimated from the distance between the COM of the C_α atoms of residues Asn296 to Phe299 of chain A and Leu64 to Val67 of chain B. Finally, Fig. 6 depicts the evolution of two H-bonds that involve Arg298. Experimental studies have indicated that they exchange during the closed-to-open transition.[33]

All the data presented in Figs. 3 to 6 were obtained using the CPPTRAJ module of the

AMBER package.[51] A pictorial description of the binding process can be found in movie S6, in the Supporting Information section. It was built with snapshots taken from the US simulations, by arranging the windows in reverse order.

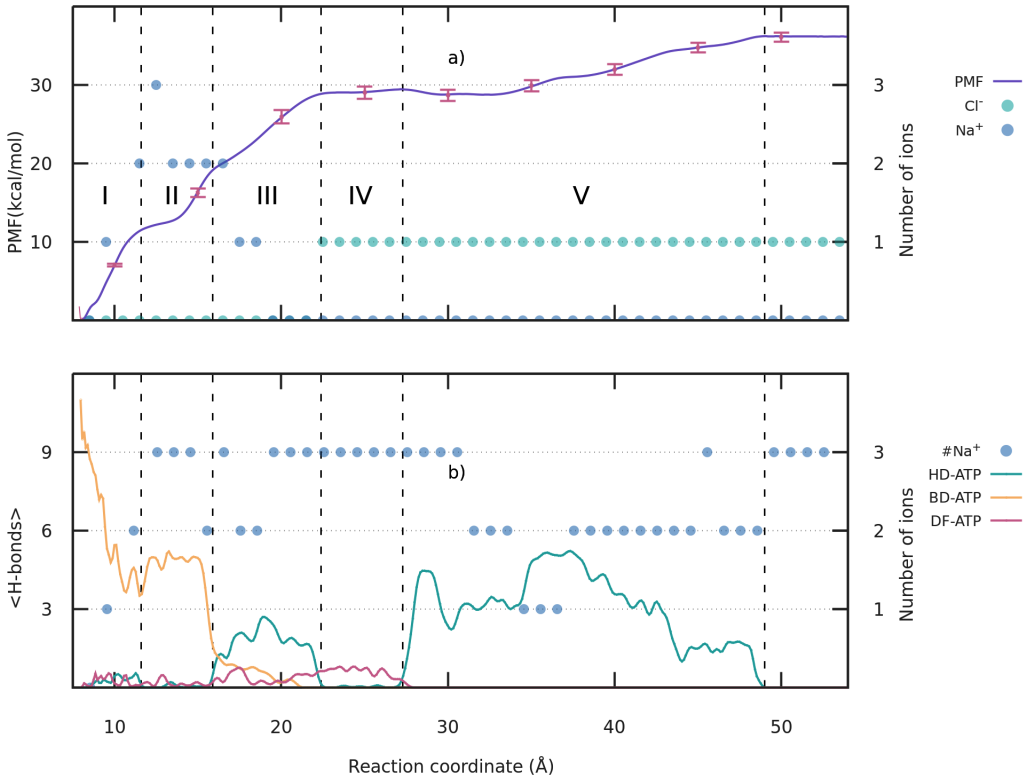

Figure 3: Evolution of parameters relevant to describe the interactions between ATP, receptor and ions, along the reaction coordinate. Panel (a) superimposes the PMF for the unbinding process (left axis) with the most likely number of Na^+ and Cl^- inside the cleft (right axis). Panel (b) superimposes the average number of H-bonds between ATP and alternative protein domains (left axis) with the most likely number of Na^+ ions interacting with ATP (right axis).

Region I

This region extends from $\chi = 8.0$ to 11.6 Å. Fig.3 shows that, at the smallest values of χ, the agonist is tightly hold inside the binding pocket interacting with residues belonging to BD of both chains via ∼11 H-bonds. They are residues Asn296, Arg298 and Lys316 of chain A and Lys70, Lys72, Lys193 and Thr189 of chain B (see Fig. 2). As can be observed in Fig. 4,

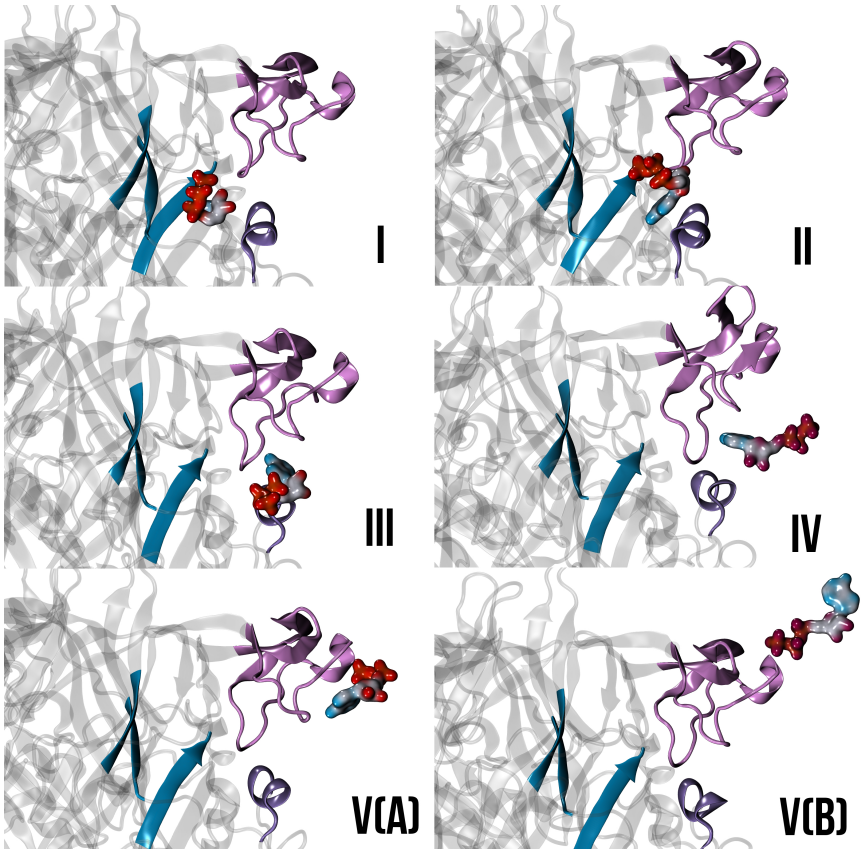

Figure 4: Conformation adopted by the ATP molecule in different regions of the reaction coordinate.The labels of the panels correspond to the regions depicted in Fig. 3. For region V we present two figures: V(A) corresponds to the shortest values of χ and V(B) to the largest values. The color in the surface of ATP indicates the electrostatic potential. It allows to distinguish the phosphate end (red) form the adenine end (light blue). Relevant domains are indicated with the same colors used in Fig. 1.

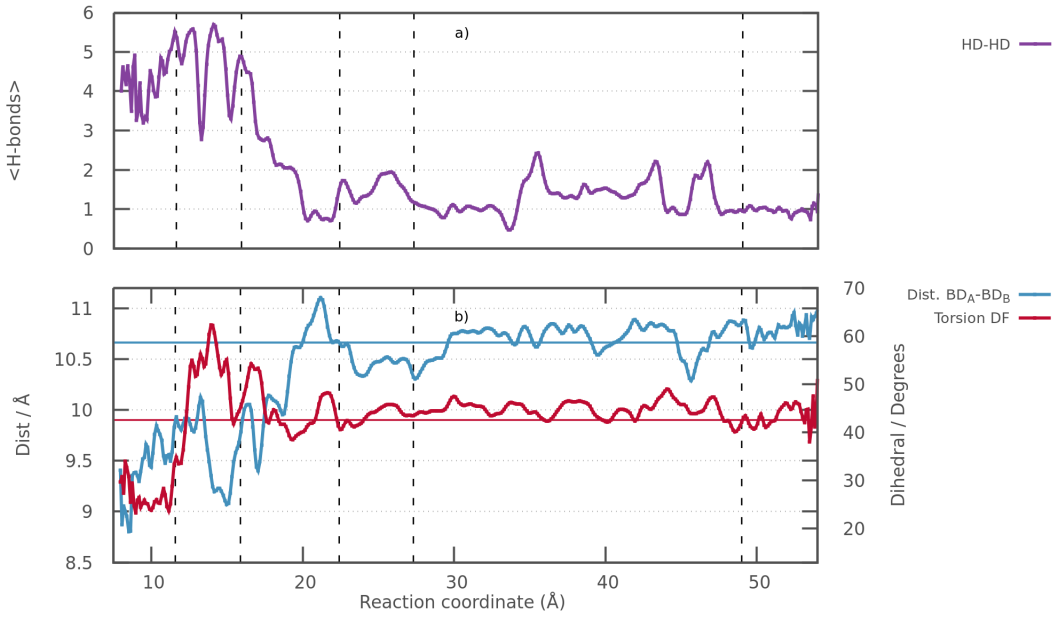

Figure 5: Evolution of parameters relevant to describe conformational changes around the binding site. Panel (a), average number of H-bonds between the loops 1 and 2 of HD. Panel (b), the left axis indicates the distance between BD of chain A and BD of chain B. The right axis indicates the value of a torsion which describes the movement of the DF of chain B (see text). The horizontal lines indicate the values of these parameters in the crystal structure of the closed conformation.

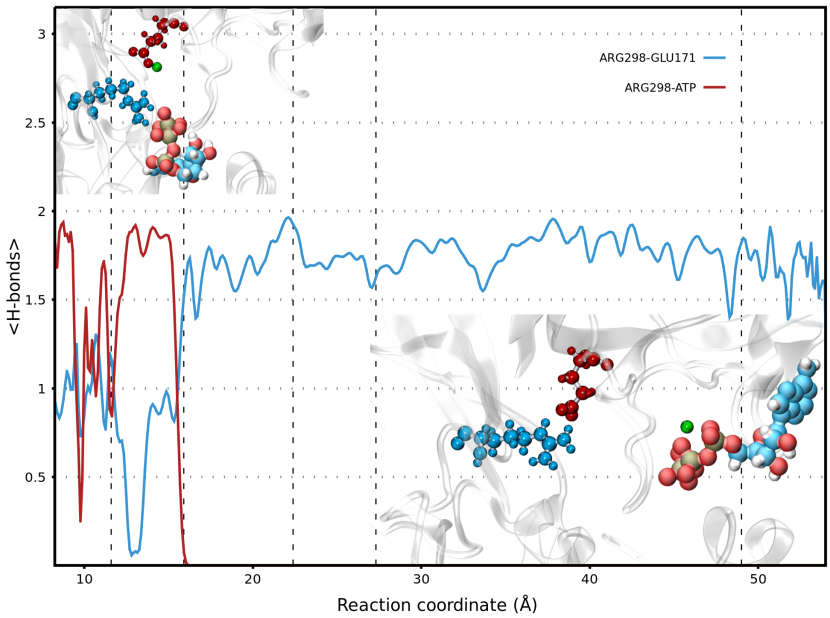

Figure 6: Evolution of salt bridges that involve Arg298. At short values of χ, Arg298 interacts with ATP. At large values of χ, Arg298 interacts with Glu171.

the ATP adopts an U-shaped conformation in which the P_γ phosphate group interacts with the -OH group at C2* of the sugar ring. At these very short values of χ there are no ions inside the cleft.

When the ATP molecule starts being withdrawn, the number of H-bonds drops to less than half of its initial value, with a concomitant increment in the free energy of $\sim$ 11.5 kcal/mol (see Fig. 3). The first interactions that get lost are those between the adenosine group and residues Asn296, Thr189 and Lys193. As a result, adenosine is released and becomes able to rotate leaving its binding pocket. In addition, the U-shaped conformation of ATP starts to evolve towards a more extended conformation.

Fig. 3 shows that, once these reorganizations have taken place, a Na^+ ion gets inside the pocket. There, it mostly interacts with the P_β and P_γ phosphate groups of ATP, but also with the carboxylic group of Glu171. The distance between the BDs of chains A and B fluctuates, but shows an overall increase within this region, from its equilibrium value of $\sim$ 8.6 Å in the bound conformation to $\sim$ 9.9 Å (see panel (b) of Fig. 5). We note that ATP is responsible for keeping BD_A and BD_B close to each other, holding each of these bodies via H-bonds with different phosphate groups. The torsion that describes the movement of DF of chain B remains almost unchanged within this region.

Region II

This region extends from $\chi = 11.6$ to 15.9 Å. Initially and up to $\chi \sim 13.8$Å, the PMF increases very slowly. After that point, it resumes a large rate of increase ending the region in $\sim$19.2 kcal/mol. In the first part, the average number of H-bonds between BD and ATP oscillates around 5, while the H-bonds with HD and DF remain very weak. However, towards the right limit of the region, the H-bonds with BD decrease to $\sim$1 while those with HD increase to $\sim$2. This overall lost of favourable interactions would explain the increase in the free energy observed at second part of this region. In parallel, we observe that the most likely number of Na^+ in the binding pocket oscillates between two and three, as indicated in panel (a) of Fig 3.

Panel (b) of the same figure shows that all these ions are interacting with the phosphate groups of ATP, which is now more exposed to the solvent. This observation reveals that the Na^+ ions facilitate the release of ATP from the binding pocket. They partially shield the negative charge of the phosphate groups, helping to break the H-bonds with positively charged residues of the body domain.

Fig. 5 shows that the torsion of DF changes dramatically within this region, reaching the maximum value observed in the whole set of simulations. This movement is required to make place for the ATP, which starts passing between DF and HD (see Fig. 4). The distance between BD_A and BD_B behaves differently in the first and second half of the region. At the beginning, it slightly oscillates around $\sim$ 9.9 Å. However, for $\chi > 13.8$ Å it firsts drops for $\sim$ 1 Å and then increases in a similar amount. In the right end of this region, the switch in the interactions of Arg298 takes place (see Fig. 6). For χ <15 Å the average number of H-bonds between this residue and ATP is $\sim$ 1.9. However, beyond that point, it markedly drops to zero. At the same time, the average number of H-bonds with Glu171 increases from 0.5 to $\sim$ 1.9 and remains like that for the rest of the unbinding process.

Region III

This section extends from $\chi = 15.9$ to 22.4 Å. As can be seen in Fig. 3a, the PMF increases steadily from $\sim$19.2 to $\sim$28.7 Å. At the beginning, the P_γ and P_β phosphate groups are still in the binding pocket while the adenine moiety points in the opposite direction, closer to HD (see Fig.4). Fig.3b demonstrates that, at the end of the range, the last H-bond between ATP and BD gets lost. This corresponds to the H-bond between the P_γ phosphate group and Lys72 of chain B. This observation reveals that this group is responsible for the most persistent interaction of the agonist in the binding site. In turn, this affords a reasonable explanation for the weak response observed when P2X receptors interact with adenosine diphosphate and adenosine monophosphate, which lack the P_γ group.[59] Once the interaction with Lys72 is broken, the three phosphate groups leave the binding pocket rotating as a rigid

body.

The average number of H-bonds between ATP and HD increases significantly at the beginning of this region, reaching a maximum of ∼2.7 in the middle of the range. Then, it starts to decrease again and becomes zero at the end. Considering the number of H-bonds between ATP and receptor altogether (BD+HD+DF), one notices that it either remains constant or slightly increases in most of the range. This observation is not consistent with the significant increase in the PMF. The inconsistency can be solved by noting that, along this region, ATP is passing between two loops of HD, disrupting several H-bond interactions between then. In regions I and II, the number of H-bonds between them oscillates between 3 and 6, with an average value of ∼4.5 (see panel (a) of Fig. 5). However, in region III, this number severely drops from almost 5 to less than 1, on average. This overall loss of favourable interactions explains the rise in the PMF.

Panel (a) of Fig. 3 shows that the presence of Na^+ in the binding pocket vanishes to zero when the phosphate groups leave the site. Panel (b) of Fig. 3 reveals that the three Na^+ ions that leave the binding pocket continue interacting with the phosphate groups of ATP until much larger values of the χ. The distance between the BDs of chains A and B presents large fluctuations within the region, but it shows an overall increase, starting at ∼9.8 Å and ending close to 11.0 Å. In turn, the torsion that describes the movement of DF decreases with some fluctuations. Towards the end of the region it starts to fluctuate around a value similar to that of the closed structure.

Region IV

This region extends from $\chi = 22.4$ to 27.3 Å. The PMF remains almost constant in the whole range. As can be seen in panel IV Fig. 4, the substrate is completely out of the binding cleft. All the H-bonds with BD and HD are broken. Only a weak H-bond with DF binds the substrate with the receptor (see Fig. 3b). The phosphate groups of ATP are completely exposed to the solvent, interacting with three Na^+. Once the phosphate groups get out, a

Cl^- gets into the pocket and locates in places previously occupied by the phosphate groups, interacting with Lys70 and Lys72 of chain B.

Figure 5 shows that the distance between BD_A and BD_B has decreased with respect to the previous region and oscillates around 10.3 Å. This value is slightly smaller than that of the closed conformation. The torsion that describes the movement of DF fluctuates around a constant value, similar to that of the closed structure. This behavior also extends to region V. This demonstrates that the conformational changes observed in the upper part of the receptor take place while ATP is leaving the binding cleft. No further changes occur when ATP interacts with residues located at the surface of HD.

Region V

This section extends from $\chi = 27.3$ to 49.0 Å. At the shortest values of χ the PMF decreases. It goes from 29.4 kcal/mol in the limit between regions IV and V to 28.5 kcal/mol at χ =32.5 Å. For χ >32.5 Å the PMF starts growing again (see Fig. 3a). We note that the energy required to escape from this shallow minimum, 0.9 kcal/mol, is pretty similar to the statistical uncertainty of the PMF, 0.7 kcal/mol. However, as can be seen in Fig. S5, this shallow minimum appears in all the alternative PMFs computed from different sets of data.

Figure 3b shows that the H-bond between ATP and DF vanishes at the beginning of this range, but several H-bonds get formed with HD. The residues involved in these interactions are Arg133, Lys136 and Arg137. The number of H-bonds between ATP and HD reaches the maximum value of 5 at $\chi = 37.3$ Å, somewhat to the right of the minimum in the free energy. We note that, when the average number of H-bonds between HD and ATP gets higher than 3, the most likely number of Na^+ interacting with ATP drops to 2 or 1. As the reaction coordinate gets larger than 37.3 Å, the interactions between ATP and HD get weaker. Close to the end, only the H-bonds with Arg133 persist. They completely vanish for $\chi > 49$ Å. When this occurs, the PMF reaches a constant value which of 36.0 kcal/mol, 7.5 kcal/mol larger than that of the minimum at χ =32.5 Å.

Results of standard MD simulations

The results of the US simulations suggest that a metastable state, in which ATP interacts with the head of the receptor, exists at the first stages of the binding process. In order to corroborate this outcome we launched 591 standard MD simulations in which a single ATP molecule was located around the extracellular part of either, the native P2X4 receptor or its triple mutant R133A/K136A/R137A. In both cases, the receptor was in the closed conformation. The protocol employed to initialize and sample these simulations was provided at the end of the previous section.

For simulations of the native form, we found that the agonist moved away from the receptor in most of the cases. However, in 27 of 591 simulations, ATP effectively attached to the head domain, while it directly attached to the entrance of the binding pocket in 6 simulations. We considered that ATP was attached when there was at least one hydrogen bond between ATP and receptor. The total number of snapshots collected in these simulations is 31700. H-bonds between ATP and HD were found in 2522 of snapshots (7.96 %) while H-bonds between ATP and residues in the entrance of the binding pocket were found in 39 (0.12%). In all cases we observed that, once the agonist adhered to the receptor, it continued attached to it for the rest of the simulation. Besides, we never saw the ATP moving from the head domain to the binding site or vice versa. Trajectories longer than 2.0 ns would be needed for that.

We found that the residues involved in the interactions with HD were, not only Arg133, Lys136 and Arg137, but also Arg151 and Lys160. However, they just appear in a small proportion of the samples (380 snapshots, 1.19% of the total). Fig S6 at the Supplementary Information section indicates the position of Arg151 and Lys160. They are in the other side of the head domain, opposite to Arg133 and Lys136. Thus, while the side chains the Arg133 and Lys136 are directed towards the entrance of the binding pocket, those of Arg151 and Lys160 point in the opposite direction. For this reason, they do not interact with ATP as it is leaving the binding pocket.

For the simulations of the triple mutant we found that ATP adhered to the head domain just 9 of 591 simulations, while it adhered to the entrance of the binding pocket in 7. Counting the snapshots, we found 282 with ATP bound to HD (0.88% of the total) and 48 attached to the binding pocket (0.15%). The H-bonds between ATP and HD involved residues Arg151 and Lys160. We therefore conclude that the fraction of events in which ATP directly attached to the entrance of the binding site or to residues Arg151 and Lys160 is similar in the native structure and the triple mutant. However, all the binding events that occur just above the entrance of the binding cleft, which are the majority in simulations of the mative structure, are lost in simulation of the triple mutant. According to this finding, we propose that the lack of Arg133, Lys136 and Arg137 should slow down the binding/unbinding process.

The VolMap plugin of VMD was used to find the places with higher ATP occupancy. In this analysis, we only employed trajectories in which ATP adhered to the receptor. More precisely, we measured the occupancy of the P atoms. Figure 7 depicts the sites with high occupancy, obtained from simulations of the native structure. Panel (a) shows a view from the side of the receptor while panel (b) shows it from above. We first note that the

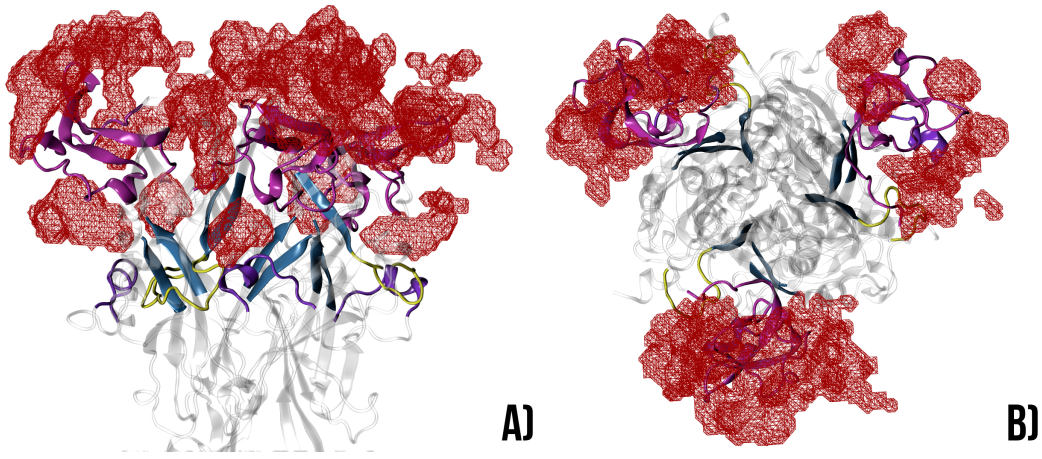

Figure 7: Sites with high occupancy probability for the P atoms of ATP. The isosurfaces indicate an occupancy probability of 0.5. Relevant domains of the receptor are indicated with the same color employed in Fig. 1. Panel (a) shows the receptor from a side while panel (b) presents a top view.

occupancy of ATP is not symmetric, as one would expect. This indicates that the sampling

of the attaching events is not converged. Trajectories of 2 ns are long enough to indicate whether ATP is going to adhere or not. In this interval, it either attaches or moves away. The problem is that, for each initial location of the ATP molecule, we run a single simulation. Full convergence requires several simulations with alternative initial conformations. In spite of this drawback, the results shown in Fig. 7 clearly depict how the agonist spontaneously attaches to the head of the native receptor. Direct attachment to the entrance of the binding cleft is also shown.

Discussion

The results presented in the previous section provide information useful to build a detailed description of the mechanism by which ATP attaches to the P2X4 receptor. Here we organize this information, in order to make explicit the mechanism.

ATP approximates the receptor interacting with 3 Na^+. When it gets near the head, it establishes H-bonds with Arg133 and loses one of the interacting cations. Once ATP is clinging to Arg133, it bends and establishes new H-bonds with Lys136 and Arg137 as well. This reduces even further the number of Na^+ around ATP. Thus, one notes that there is always a competition between positively charged residues of the receptor and Na^+ ions, to interact with the phosphate groups of ATP. This conclusion can be obtained from the analysis of Fig. 3, but can also be observed in Movie S6.

When the reaction coordinate gets slightly shorter, Na^+ ions approximate the phosphate groups, debilitating their H-bonds with HD. Eventually, ATP starts detaching from HD and moves down. In this movement, it establishes a weak and transient H-bond with residues Ser215 and Thr218 of DF. This is clearly shown in movie S6. Finally, the agonist locates between HD and DF and establishes new H-bond interactions with HD.

At this point, the agonist starts moving into the cleft. As it does so, it displaces any Cl^- located inside and drags into the cleft the three Na^+ attached to it. An important effect

observed at this point is that several H-bonds between the two loops of HD get formed as the ATP moves in. The average number of H-bonds between them variates from ∼1 to nearly 5 as χ goes from 22.4 Å to 15.9 Å (see Fig. 3b). This causes a reduction in the PMF of almost 9.5 kcal/mol. Once reached the value of $\chi = 15.9$ Å, the number of H-bonds between the two loops oscillates around an average of 4.5 and remains like that for the rest of the process. The distance between BD_A and BD_B initially increases from the values corresponding to the closed receptor up to 11.1 Å, but then decreases to oscillate around 10 Å, a value similar to that observed when ATP is completely bound.

When the reaction coordinate decreases to less than 15.9 Å, the H-bonds between HD and ATP disappear, but this loss is more than compensated by almost 4 new H-bonds between BD and ATP. This causes another significant reduction in the PMF which goes from 19.1 to 11.3 kcal/mol. Among the new H-bonds are those between ATP and Arg298, which disrupt the interaction of Arg298 and Glu171. In order to allow the entrance of ATP, DF has to rotate. The torsional angle that measures this movement increases from 42° at $\chi = 15.7$ Å to 62° at $\chi = 14.1$ Å . Then, it decreases again. Its minimum value of ∼26° is attained close to the minimum of the PMF.

When the reaction coordinate gets smaller than 11 Å new H bonds between BD and ATP are created. The average number increases from 4 to 11. The PMF reduces in ∼11.5 kcal/mol to reach its minimum value at χ =8.1 Å. As the number of H-bonds between ATP and BD increases, the number of Na^+ attached to the phosphate groups reduced. At the equilibrium position of the bound state there are no Na^+ in the binding cleft.

Previous studies have addressed the head domain of P2X4 receptors as a putative place for the docking of inhibitors.[60,61] Several binding sites for inhibitory divalent cations were detected in rat P2X4.[60] More recently, an affinity-optimized negatively-charged antibody that completely inhibits hP2X4, was produced. It was determined that residue K127 is crucial for the inhibitory activity of this antibody.[61] We note that this residue is not conserved in zfP2X4, and the similarity of both sequences is rather low in the region of HD. Aside from

these previous studies on inhibitors, we did not find any report in which the relevance for ATP binding, of positively charged residues in the head domain of p2x4, has been discussed.

Conclusions

We have studied the binding/unbinding of an ATP molecule from the open P2X4 receptor, using Umbrella Sampling and standard molecular dynamics simulations. The analysis of the results has revealed the sequence of conformational changes that occur during the reversible binding of ATP and provided information about the interactions that develop throughout the course of the process. Among these, it stands out the initial attachment of ATP to the head domain of the receptor. This occurs in the first stages of the binding process and involves residues Arg133, Lys136 and Arg137. To the best of our knowledge, the role played by these residues has not been highlighted before. We hope the findings reported in this article can call the attention of research groups able to do experiments aimed to confirm or refuse in our results.

Acknowledgement

The authors thank to the High Performance Computing Center (CeCAR) of the University of Buenos Aires for allowing us to use their computational facilities. This work was supported by the Universidad Nacional de Quilmes (ID:1358/17), CONICET (ID:11220130100260CO) and ANPCyT (ID:2436).

Supporting Information Available

This information is available free of charge via the Internet at http://pubs.acs.org.

- Model construction. A piece of text detailing the procedure employed to build the computational model for the open P2X4 receptor.

- Fig. S1 shows the initial locations of the ATP molecule in 591 standard molecular dynamics simulations used to identify the locations where ATP adheres to the receptor.
- Fig. S2 compares the PMFs obtained with WHAM and DHAM.
- Fig. S3 depicts typical examples of function $F_i(\chi)$, defined in Eq. 1 of the main text, in four pairs of adjacent windows.
- Fig. S4 shows the variation of the Symmetric Kullback-Leibler divergence S_i as a function of the reaction coordinate (see Eq. 3 of the main text).
- Fig. S5 presents four alternative PMFs computed from different sets of data.
- Fig. S6 depicts the position of Arg151 and Lys160 with respect to Arg133, Lys136 and Arg137.
- Movie S6 pictorically illustrates the reversible binding of ATP to the P2X4 receptor.

References

(1) Khakh, B. S.; North, R. A. P2X Receptors as Cell-Surface ATP Sensors in Health and Disease. *Nature* **2006**, *442*, 527–532.

(2) Browne, L.; Jiang, L.-H.; North, A. New Structure Enlivens Interest in P2X Receptors. *Trends in Pharmacological Sciences* **2010**, *31*, 229–237.

(3) Bean, B. ATP-Activated Channels in Rat and Bullfrog Sensory Neurons: Concentration Dependence and Kinetics. *The J. Neurosci.* **1990**, *10*, 1–10.

(4) Nicke, A.; Hans, B.; Jürgen, R.; Eichele, A.; Günter, L.; Ernst, M.; Günter, S. P2X1 and P2X3 Receptors Form Stable Trimers: a Novel Structural Motif of Ligand-Gated Ion Channels. *EMBO J.* **1998**, *17*, 3016–3028.

(5) Surprenant, A.; North, R. A. Signaling at Purinergic P2X Receptors. *Annu. Rev. Physiol.* **2009**, *71*, 333–359.

(6) Edwards, F. A.; Gibb, A. J.; Colquhoun, D. ATP Receptor-Mediated Synaptic Currents in the Central Nervous System. *Nature* **1992**, *359*, 144–147.

(7) Khakh, B. S.; Henderson, G. ATP Receptor-Mediated Enhancement of Fast Excitatory Neurotransmitter Release in the Brain. *Mol. Pharmacol.* **1998**, *54*, 372–378.

(8) Finger, T. E.; Danilova, V.; Barrows, J.; Bartel, D. L.; Vigers, A. J.; Stone, L.; Hellekant, G.; Kinnamon, S. C. ATP Signaling Is Crucial for Communication from Taste Buds to Gustatory Nerves. *Science* **2005**, *310*, 1495–1499.

(9) Cook, S. P.; Vulchanova, L.; Hargreaves, K. M.; Elde, R.; McCleskey, E. W. Distinct ATP Receptors on Pain-Sensing and Stretch-Sensing Neurons. *Nature* **1997**, *387*, 505–508.

(10) Cockayne, D. A.; Hamilton, S. G.; Zhu, Q.-M.; Dunn, P. M.; Zhong, Y.; Novakovic, S.; Malmberg, A. B.; Cain, G.; Berson, A.; Kassotakis, L.; Hedley, L.; Lachnit, W. G.; Burnstock, G.; McMahon, S. B.; Ford, A. P. D. W. Urinary Bladder Hyporeflexia and Reduced Pain-Related Behaviour in P2X3-Deficient Mice. *Nature* **2000**, *407*, 1011–1015.

(11) Galligan, J. J. Enteric P2X Receptors as Potential Targets for Drug Treatment of the Irritable Bowel Syndrome. *Br. J. Pharmacol.* **2004**, *141*, 1294–1302.

(12) Miller, C. M.; Boulter, N. R.; Fuller, S. J.; Zakrzewski, A. M.; Lees, M. P.; Saunders, B. M.; Wiley, J. S.; Smith, N. C. The Role of the P2X7 Receptor in Infectious Diseases. *PLoS Pathog* **2011**, *7*, e1002212.

(13) Chessell, I. P.; Hatcher. J. P.; Bountra, Chas.; Michel, Anton. D.; Hughes, J. P.; Green, P.; Egerton, J.; Murfin, M.; Richardson, J.; Peck, W. L.; Grahames, C. B. A.;

Casula, M. A.; Yiangou, Y.; Birch, R.; Anand, P.; Buell, G. N. Disruption of the P2X7 Purinoceptor Gene Abolishes Chronic Inflammatory and Neuropathic Pain. *Pain* **2005**, *114*, 386–396.

(14) Fabre, J.; Nguyen, M.; Latour, A.; Keifer, J. A.; Audoly, L. P.; Coffman, T.; Koller, B. H. Decreased Platelet Aggregation, Increased Bleeding Time and Resistance to Thromboembolism in P2Y1-Deficient Mice. *Nat. Med.* **1999**, *5*, 1199–2012.

(15) Romagnoli, R.; Baraldi, P. G.; Cruz-Lopez, O.; Lopez-Cara, C.; Preti, D.; Borea, P. A.; Gessi, S. The P2X7 Receptor as a Therapeutic Target. *Expert Opinion on Therapeutic Targets* **2008**, *12*, 647–661.

(16) Burnstock, G.; Kennedy, C. P2X Receptors in Health and Disease. *Adv Pharmacol* **2011**, *61*, 333–372.

(17) Jelassi, B.; Chantme, A.; Alcaraz-Pérez, F.; Baroja-Mazo, A.; Cayuela, M. L.; Pelegrin, P.; Surprenant, A.; Roger, S. P2X7 Receptor Activation Enhances SK3 Channels and Cystein Cathepsin-Dependent Cancer Cells Invasiveness. *Oncogene* **2011**, *30*, 2108–2122.

(18) Adinolfi, E.; Capece, M.; Amoroso, F.; Marchi, E. D.; Franceschini, A. Emerging Roles of P2X Receptors in Cancer. *Curr. Med. Chem.* **2015**, *22*, 878–890.

(19) North, R. A.; Jarvis, M. F. P2X Receptors as Drug Targets. *Mol. Pharmacol.* **2013**, *83*, 759–769.

(20) North, R. A. Molecular Physiology of P2X Receptors. *Physiological Reviews* **2002**, *82*, 1013–1067.

(21) Kawate, T.; Michel, J. C.; Birdsong, W. T.; Gouaux, E. Crystal Structure of the ATP-Gated P2X4 Ion Channel in the Closed State. *Nature* **2009**, *460*, 592–598.

(22) Hattori, M.; Gouaux, E. Molecular Mechanism of ATP Binding and Ion Channel Activation in P2X Receptors. *Nature* **2012**, *485*, 207–212.

(23) Mansoor, S. E.; L, W.; Oosterheert, W.; Shekhar, M.; Tajkhorshid, E.; Gouaux, E. X-ray Structures Define Human P2X3 Receptor Gating Cycle and Antagonist Action. *Nature* **2016**, *538(7623)*, 66–71.

(24) Wang, J.; Wang, Y.; Cui, W.-W.; Huang, Y.; Yang, Y.; Liu, Y.; Zhao, W.-S.; Cheng, X.-Y.; Sun, W.-S.; Cao, P.; Zhu, M. X.; Wang, R.; Hattori, M.; Yu, Y. Druggable Negative Allosteric Site of P2X3 Receptors. *PNAS* **2018**, *115*, 4939–4944.

(25) Karasawa, A.; Kawate, T. Structural Basis for Subtype-specific Inhibition of the P2X7 Receptor. *eLife* **2016**, *5*, e22153.

(26) Kasuya, G.; Yamaura, T.; Ma, X.-B.; Nakamura, R.; Takemoto, M.; Nagumo, H.; Tanaka, E.; Dohmae, N.; Nakane, T.; Yu, Y.; Ishitani, R.; Matsuzaki, O.; Hattori, M.; Nureki, O. Structural Insights into the Competitive Inhibition of the ATP-gated P2X Receptor Channel. *Nat. Commun.* **2017**, *8*, 876.

(27) McCarthy, A.; Yoshioka, C.; Mansoor, S. Full-Length P2X7 Structures Reveal How Palmitoylation Prevents Channel Desensitization. *Cell* **2019**, *179*, 659–670.

(28) Roberts, J. A.; Evans, R. J. Contribution of Conserved Polar Glutamine, Asparagine and Threonine Residues and Glycosylation to Agonist Action at Human P2X1 Receptors for ATP. *J. Neurochem.* **2006**, *96*, 843–852.

(29) Ennion, S.; Hagan, S.; Evans, R. J. The Role of Positively Charged Amino Acids in ATP Recognition by Human P2X1 Receptors. *J. Biol. Chem.* **2000**, *275*, 35656.

(30) Ennion, S. J.; Ritson, J.; Evans, R. J. Conserved Negatively Charged Residues Are Not Required for ATP Action at P2X1 Receptors. *Biochem. Biophys. Res. Commun.* **2001**, *289*, 700 – 704.

(31) Gasparri, F.; Wengel, J.; Grutter, T.; Pless, S. A. Molecular Determinants for Agonist Recognition and Discrimination in P2X2 Receptors. *J. Gen. Physiol.* **2019**,

(32) Chataigneau, T.; Lemoine, D.; Grutter, T. Exploring the ATP-binding site of P2X receptors. Front. Cell. Neurosci. 2013.

(33) Hausmann, R.; Günther, J.; Kless, A.; Kuhlmann, D.; Kassack, M. U.; Bahrenberg, G.; Markwardt, F.; Schmalzing, G. Salt Bridge Switching from Arg290/Glu167 to Arg290/ATP Promotes the Closed-to-Open Transition of the P2X2 Receptor. *Mol. Pharmacol.* **2013**, *83*, 73–84.

(34) Khakh, B. S.; North, R. A. Neuromodulation by Extracellular ATP and P2X Receptors in the CNS. *Neuron* **2012**, *76*, 51–69.

(35) Hausmann, R.; Kless, A.; Schmalzing, G. Key Sites for P2X Receptor Function and Multimerization: Overview of Mutagenesis Studies on a Structural Basis. *Curr. Med. Chem.* **2015**, *22*, 799–818.

(36) Pierdominici-Sottile, G.; Moffatt, L.; Palma, J. The Dynamic Behavior of the P2X4 Ion Channel in the Closed Conformation. *Biophys. J.* **2016**, *111*, 2642–2650.

(37) Huang, L.-D.; Fan, Y.-Z.; Tian, Y.; Yang, Y.; Liu, Y.; Wang, J.; Zhao, W.-S.; Zhou, W.-C.; Cheng, X.-Y.; Cao, P.; Lu, X.-Y.; Yu, Y. Inherent Dynamics of Head Domain Correlates with ATP-Recognition of P2X4 Receptors: Insights Gained from Molecular Simulations. *PLoS ONE* **2014**, *9*, e97528.

(38) Du, J.; Dong, H.; Zhou, H.-X. Gating Mechanism of a P2X4 Receptor Developed from Normal Mode Analysis and Molecular Dynamics Simulations. *PNAS* **2012**, *109*, 4140–4145.

(39) Pierdominici-Sottile, G.; Racigh, V.; Ormazbal, A.; Palma, J. Charge Discrimination

in P2X4 Receptors Occurs in Two Consecutive Stages. *J. Phys. Chem. B* **2019**, *123*, 1017–1025.

(40) Kawate, T.; Robertson, J. L.; Li, M.; Silberberg, S. D.; Swartz, K. J. Ion Access Pathway to the Transmembrane Pore in P2X Receptor Channels. *J. Gen. Physiol.* **2011**, *137*, 579–590.

(41) Li, M.; Wang, Y.; Banerjee, R.; Marinelli, F.; Silberberg, S.; Faraldo-Gmez, J. D.; Hattori, M.; Swartz, K. J. Molecular Mechanisms of Human P2X3 Receptor Channel Activation and Modulation by Divalent Cation Bound ATP. *eLife* **2019**, *8*, e47060.

(42) Heymann, G.; Dai, J.; Li, M.; Silberberg, S. D.; Zhou, H.-X.; Swartz, K. J. Inter and Intrasubunit Interactions Between Transmembrane Helices in the Open State of P2X Receptor Channels. *PNAS* **2013**, *110*, 4045–4054.

(43) Li, G.-H. Exploring Conformational States and Helical Packings in the P2X Receptor Transmembrane Domain by Molecular Dynamics Simulation. *J. Biol. Phys.* **2018**, *44*, 331–344.

(44) Li, G.-H. Geometric Rules of Channel Gating Inferred from Computational Models of the P2X Receptor Transmembrane Domain. *J. Mol. Graphics Modell.* **2015**, *61*, 107 – 114.

(45) Wang, J.; Wang, Y.; Cui, W.-W.; Huang, Y.; Yang, Y.; Liu, Y.; Zhao, W.-S.; Cheng, X.-Y.; Sun, W.-S.; Cao, P.; Zhu, M. X.; Wang, R.; Hattori, M.; Yu, Y. Druggable Negative Allosteric Site of P2X3 Receptors. *PNAS* **2018**, *115*, 4939–4944.

(46) Zhao, W.-S.; Wang, J.; juan Ma, X.; Yang, Y.; Liu, Y.; dong Huang, L.; Fan, Y.-Z.; Cheng, X.; zhuan Chen, H.; Wang, R. I.; Yu, Y. J. Relative Motions Metween Left Flipper and Dorsal Fin Domains Favour P2X4 Receptor Activation. *Nat. Commun.* **2014**, *5*, 4189.

(47) Jo, S.; Lim, J.; Klauda, J. B.; Im, W. CHARMM-GUI Membrane Builder for Mixed Bilayers and its Application to Yeast Membranes. *Biophys. J.* **2009**, *97*, 50–58.

(48) Wu, E. L.; Cheng, X.; Jo, S.; Rui, H.; Song, K. C.; Dvila-Contreras, E. M.; Qi, Y.; Lee, J.; Monje-Galvan, V.; Venable, R. M.; Klauda, J. B.; Im, W. CHARMM-GUI Membrane Builder Toward Realistic Biological Membrane Simulations. *J. Comput. Chem.* **2014**, *35*, 1997–2004.

(49) Hornak, V.; Abel, R.; Okur, A.; Strockbine, B.; Roitberg, A.; Simmerling, C. Comparison of Multiple Amber Force Fields and Development of Improved Protein Backbone Parameters. *Proteins: Struct., Funct., Bioinf.* **2006**, *65*, 712–725.

(50) Dickson, C. J.; Madej, B. D.; Skjevik, A. A.; Betz, R. M.; Teigen, K.; Gould, I. R.; Walker, R. C. Lipid14: The Amber Lipid Force Field. *J. Chem. Theory Comput.* **2014**, *10*, 865–879.

(51) Case, D. .A.; Darden, T. A.; Cheatham, T. E.; Simmerling, C. L.; Wang, J.; Duke, R. E.; Luo, R.; Walker, R. C.; Zhang, W.; Merz, K. M.; Roberts, B.; Hayik, S.; Roitberg, A.; Seabra, G.; Swails, J.; Goetz, A. W.; Kolossvry, I.; Wong, K. F.; Paesani, F.; Vanicek, J.; Wolf, R. M.; Liu, J.; Wu, X.; Brozell, S. R.; Steinbrecher, T.; Gohlke, H.; Cai, Q.; Ye, X.; Wang, J.; Hsieh, M. J.; Cui, G.; Roe, D. R.; Mathews, D. H.; Seetin, M. G.; Salomon-Ferrer, R.; Sagui, C.; Babin, V.; Luchko, T.: Gusarov, S.; Kovalenko, A.; Kollman, P. A. Amber16, Reference Manual. 2016.

(52) Darden, T.; York, D.; Pedersen, L. Particle Mesh Ewald: An N.log(N) Method for Ewald Sums in Large Systems. *J. Chem. Phys.* **1993**, *98*, 10089–10092.

(53) Essmann, U.; Perera, L.; Berkowitz, M. L.; Darden, T.; Lee, H.; Pedersen, L. G. A Smooth Particle Mesh Ewald Method. *J. Chem. Phys.* **1995**, *103*, 8577–8593.

(54) Kästner, J. Umbrella sampling. *Wiley Interdisciplinary Reviews: Computational Molecular Science* **2011**, *1*, 932–942.

(55) Zhu, F.; Hummer, G. Convergence and Error Estimation in Free Energy Calculations Using the Weighted Histogram Analysis Method. *J. Comput. Chem.* **2012**, *33*, 453–465.

(56) Kumar, S.; Rosenberg, J. M.; Bouzida, D.; Swendsen, R. H.; Kollman, P. A. The Weighted Histogram Analysis Method for Free-Energy Calculations on Biomolecules. I. The Method. *J. Comput. Chem.* **1992**, *13*, 1011–1021.

(57) Rosta, E.; Hummer, G. Free Energies from Ddynamic Weighted Histogram Analysis Using Unbiased Markov State Model. *J. Chem. Theory Comput.* **2014**, *11*, 276–285.

(58) Pohorille, A.; Jarzynski, C.; Chipot, C. Good Practices in Free-Energy Calculations. *J. Phys. Chem. B* **2010**, *114*, 10235–10253.

(59) Gever, J. R.; Cockayne, D. A.; Dillon, M. P.; Burnstock, G.; Ford, A. P. D. W. Pharmacology of P2X Channels. *Pflugers Arch.* **2006**, *452*, 513–537.

(60) Igawa, T.; Abe, Y.; Tsuda, M.; Inoue, K.; Ueda, T. Solution Structure of the Rat P2X4 Receptor Head Domain Involved in Inhibitory Metal Binding. *FEBS Lett.* **2015**, *589*, 680–686.

(61) Williams, W. et al. Antibodies Binding the Head Domain of P2X4 Inhibit Channel Function and Reverse Neuropathic Pain. *Pain* **2019**, *160*, 1989–2003.

Graphical TOC Entry